

SD-FSMIS: Adapting Stable Diffusion for Few-Shot Medical Image Segmentation

Meihua Li^{1†}, Yang Zhang^{1†*}, Weizhao He¹, Hu Qu¹, Yisong Li¹

¹Computer Vision Institute, College of Computer Science and Software Engineering, Shenzhen University

limeihua2023@email.szu.edu.cn, yangzhang@szu.edu.cn, heweizhao2022@email.szu.edu.cn, {quhu, liyisong}2023@email.szu.edu.cn

Abstract

Few-Shot Medical Image Segmentation (FSMIS) aims to segment novel object classes in medical images using only minimal annotated examples, addressing the critical challenges of data scarcity and domain shifts prevalent in medical imaging. While Diffusion Models (DM) excel in visual tasks, their potential for FSMIS remains largely unexplored. We propose that the rich visual priors learned by large-scale DMs offer a powerful foundation for a more robust and data-efficient segmentation approach. In this paper, we introduce SD-FSMIS, a novel framework designed to effectively adapt the powerful pre-trained Stable Diffusion (SD) model for the FSMIS task. Our approach repurposes its conditional generative architecture by introducing two key components: a Support-Query Interaction (SQI) and a Visual-to-Textual Condition Translator (VTCT). Specifically, SQI provides a straightforward yet powerful means of adapting SD to the FSMIS paradigm. The VTCT module translates visual cues from the support set into an implicit textual embedding that guides the diffusion process, enabling precise conditioning of the generation process. Extensive experiments demonstrate that SD-FSMIS achieves competitive results compared to state-of-the-art methods in standard settings. Surprisingly, it also demonstrated excellent generalization ability in more challenging cross-domain scenarios. These findings highlight the immense potential of adapting large-scale generative models to advance data-efficient and robust medical image segmentation.

1. Introduction

With the rapid advancement of artificial intelligence [12, 13, 22, 27, 41, 42, 51], automated medical image segmentation has emerged as a cornerstone technology, playing a crucial role in a multitude of clinical applications [29, 36]. It empowers early disease detection and facilitates treat-

[†]Equal Contribution: Meihua Li and Yang Zhang

^{*}Corresponding Author: Yang Zhang

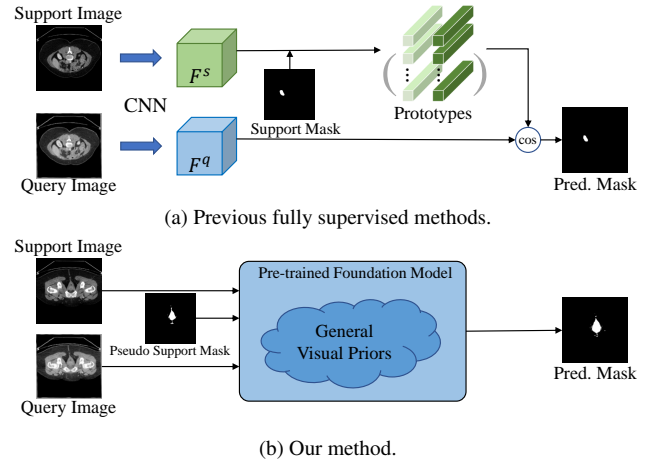


Figure 1. Comparison between our proposed method and previous methods. (a) Previous fully supervised methods build task-specific networks from scratch and require pixel-level annotations. They generate class prototypes from the limited support set and perform segmentation via feature matching. Lacking strong priors and trained on constrained data, these models are often brittle and struggle with complex visual variations. (b) Instead of building a new network, we adapt a powerful pre-trained foundation model and do not rely on manual annotations. Our framework steers its vast, generalizable visual priors, achieving superior robustness and generalization, especially in challenging cross-domain scenarios.

ment planning tailored to individual patient characteristics, thereby advancing the frontier of personalized healthcare. However, the remarkable success of these deep learning-based models is critically dependent on vast, meticulously annotated datasets for training. This dependency presents a significant real-world obstacle: acquiring large-scale, high-quality, pixel-level annotations across diverse medical domains is notoriously difficult, prohibitively expensive, and exceptionally time-consuming. Furthermore, the clinical deployment of these models is often plagued by detrimental domain shifts, arising from variations in imaging protocols, scanner types, anatomical presentations, or pathologies unseen during training.

Fortunately, Few-Shot Learning (FSL) has emerged as a promising paradigm to address this data scarcity. FSL aims to train a model capable of recognizing and generalizing to novel classes using only a limited number of labeled examples. Consequently, researchers have extended this breakthrough to the medical imaging domain, giving rise to Few-Shot Medical Image Segmentation (FSMIS) [5, 52] to mitigate the aforementioned challenges. Despite advances driven by meta-learning and prototype-based networks, achieving robust and data-efficient performance remains a significant challenge, especially against the complex and heterogeneous backdrop of medical imaging. The majority of conventional FSMIS approaches still focus on designing more elaborate matching networks, such as those leveraging prototypical networks and attention mechanisms, as illustrated in Fig. 1a. Such models, however, are often constrained by their inherent architectural limitations, leading to a performance drop when encountering complex or unseen variations. This brittleness severely limits their clinical utility and robustness.

To bridge this critical generalization gap, we advocate for a paradigm shift, conceptually depicted in Fig. 1b. Instead of designing increasingly complex, task-specific architectures trained on limited data, we propose to leverage the powerful and generalizable visual priors encapsulated within large-scale pre-trained foundation models. Diffusion Models (DMs) [6], which have achieved remarkable success not only in generative tasks [25] but have also demonstrated immense potential in fundamental vision tasks like pixel-level prediction [1, 49] and semantic correspondence [14, 50]. This potential stems from their ability to learn rich, generalizable representations of texture, shape, and context from massive, diverse datasets such as LAION-5B [32]. While these learned priors offer tremendous potential for understanding visual structure, their application to dense prediction tasks like FSMIS remains largely unexplored.

In this paper, we introduce SD-FSMIS, a novel framework that adapts a powerful pre-trained Stable Diffusion (SD) [30] model to address the core challenges of FSMIS and enhance its resilience against the complexities of medical imaging. Our central objective is to explore how to efficiently and directly adapt the general-purpose visual priors of SD to serve the FSMIS task. We achieve this through two primary architectural innovations: (1) Support-Query Interaction (SQI), which facilitates effective information exchange in the latent space. By minimally modifying the self-attention layers of the SD model, SQI propagates class-specific information from the support set to the query image, seamlessly adapting SD to the few-shot segmentation paradigm. (2) Visual-to-Textual Condition Translator (VTCT), which acts as a "visual-to-semantic" translator. This module converts class-specific visual information from

the support set into implicit text-like embeddings. This allows us to precisely condition the SD model using the "language" it understands, steering its powerful generative priors to focus on the desired anatomical structures while maximally reusing its existing components.

In summary, our main contributions are:

- We propose a new paradigm for FSMIS that leverages the rich, generalizable visual priors from pre-trained text-to-image diffusion models to tackle the critical challenge of cross-domain generalization. This shifts the focus from designing task-specific networks from scratch to effectively adapting powerful foundation models.
- We introduce SD-FSMIS, a novel yet minimalist adaptation framework. It features the Support-Query Interaction (SQI) module for latent-space fusion and the Visual-to-Textual Condition Translator (VTCT) module, which translates visual cues into text-like conditioning signals to precisely guide the diffusion model.
- Extensive experiments demonstrate that our method not only achieves competitive performance in standard FSMIS settings but, more importantly, significantly outperforms state-of-the-art methods in challenging cross-domain scenarios. This empirically validates the superior generalization and robustness of our approach in handling the complex and variable nature of medical imaging.

2. Related Work

Few-Shot Semantic Segmentation. Few-shot semantic segmentation (FSS) aims to perform dense pixel-level prediction for novel classes guided by a minimal set of annotated support images. The field has been largely shaped by two dominant research thrusts. The most influential is the prototype-matching paradigm. Pioneered by early works [8, 33], this approach generates a representative class prototype from the support set's features, which then guides the segmentation of the query image through a similarity matching process. Subsequent research has focused on refining this core idea; for instance, by creating more discriminative representations through multiple region-aware prototypes [52] or by improving the metric learning space [19, 40]. A parallel line of research concentrates on enhancing the interaction between support and query features. These methods aim to achieve a deeper fusion between the two branches, for example, by generating prior maps and leveraging multi-scale feature alignment to enrich the query representation before the final prediction [39].

Few-Shot Medical Image Segmentation. The principles of FSS have been adapted to the unique constraints of medical imaging, where pronounced data scarcity and domain heterogeneity are the norms. Existing FSMIS research largely mirrors the trends in FSS, primarily evolving along two axes. One line of work refines the prototype-matching paradigm to handle the nuances of medical data. Innova-

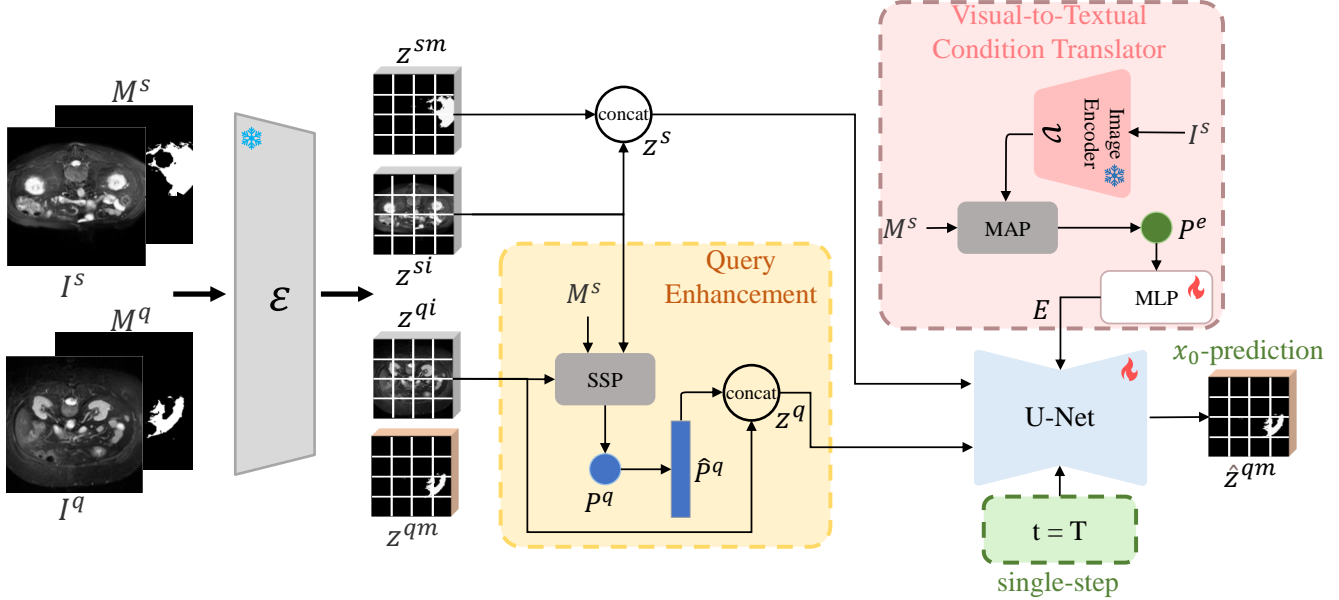


Figure 2. SD-FSMIS Overview and Training Pipeline. Support and query sets are first encoded using the VAE encoder \mathcal{E} . The query latent z^{qi} is enhanced via the Query Enhancement module to obtain z^q , while the support latent z^{si} and its mask latent z^{sm} are concatenated along the channel dimension to form z^s . These are then fed into the U-Net, where the query mask latent \hat{z}^{qm} is generated under the condition of the text embedding E , produced by the Visual-to-Textual Condition Translator module.

tions include generating adaptive local prototypes to better capture anatomical variability [28], and introducing learnable thresholds to improve the robustness of the matching process against complex backgrounds [11, 34]. A parallel effort focuses on designing more elaborate dual-branch interaction mechanisms. These methods employ improved attention or recurrent modules to explicitly model and calibrate the feature-level correlations between support and query images [7, 10, 31]. In this more realistic scenario, the model is tested on target classes and data distributions entirely unseen during training. The difficulty of CD-FSMIS, which is the true litmus test for clinical applicability, underscores the critical need for models endowed with powerful, pre-existing visual priors that are not confined to a narrow medical distribution.

Diffusion Models. Diffusion models have demonstrated remarkable capabilities across various visual generation tasks. Researchers have extensively explored their visual features, applying them to zero-shot classification [21], supervised segmentation [1], label-efficient segmentation [2], semantic correspondence matching [14, 50], and open-vocabulary segmentation [49]. These models typically employ Latent Diffusion Models (LDM) [30], which compress images into latent space, significantly reducing computational costs and enabling the first open-source text-to-image diffusion model at LAION-5B [32] scale. Recent research has shown increasing interest in diffusion-based segmentation methods [22, 46, 47, 51], which generate segmentation pre-

dictions based on image conditions. Diffusion models have exhibited substantial potential in fine-grained pixel prediction [20, 48] and semantic correspondence tasks [24, 38]. Notably, SDSeg [22] developed a medical image segmentation approach based on LDM, while DiffewS [51] introduced diffusion models to Few-Shot Segmentation, leveraging generative framework priors to maximize task performance.

3. Methodology

3.1. Problem Formulation

Few-shot semantic segmentation aims to train a model capable of segmenting novel class images using a minimal number of labeled data, without model retraining. Specifically, the training set D_{train} comprises a base class set C_{train} with sufficient annotated samples, and the test set D_{test} includes a novel class set C_{test} with a limited number of annotated samples, where $C_{train} \cap C_{test} = \emptyset$.

We follow the episode-based training approach commonly used in few-shot semantic segmentation tasks [40]. The training and testing sets are divided into multiple episodes, each containing a support set S and a corresponding query set Q with the same class. The support set for each class contains K image-mask pairs, denoted as $S = \{(I_s^i, M_s^i)\}_{i=1}^K$, with the corresponding query set represented as $Q = (I^q, M^q)$. Here, $I \in \mathbb{R}^{H \times W \times 1}$ represents grayscale images, and $M \in \{0, 1\}^{H \times W}$ represents corre-

sponding binary masks. We learn class information from the support set S and then predict masks for query images.

Following ADNet [11], we adopt a 1-way 1-shot meta-learning strategy for FSMIS. Additionally, we utilize the supervoxel clustering method proposed by ADNet to generate pseudo-labels as training annotations. This approach allows us to better leverage the volumetric characteristics of medical images and eliminate the need for explicit data labeling.

3.2. Network Architecture

To apply Stable Diffusion to FSMIS, we introduce a novel approach called SD-FSMIS. The overall architecture, illustrated in Fig. 2, comprises two primary novel components: a Support-Query Interaction (SQI) module and a Visual-to-Textual Condition Translator (VTCT) module, which orchestrate the few-shot learning process. The core of our network leverages the powerful generative prior learned by Stable Diffusion, originally trained on the large-scale LAION-5B dataset. We introduce minimal, targeted modifications to adapt its components into an effective few-shot segmentation framework.

VAE Encoder and Decoder. We utilize the pre-trained VAE component of Stable Diffusion to map images and masks into a shared latent space, where the conditional denoising process occurs. The VAE weights are kept frozen throughout our training, preserving the rich visual features learned during its original training. We investigate the reconstruction capabilities of VAE for both medical images and binary masks in the supplementary materials. A key challenge is adapting the VAE, designed for 3-channel RGB inputs, to handle single-channel medical images and their corresponding binary segmentation masks. To address this, we replicate both the input image and the mask across three channels, creating pseudo-RGB representations. Furthermore, pixel values of both image and mask are normalized to the range $[-1, 1]$ to align with the VAE’s expected input distribution. During inference, after the diffusion process yields a latent representation of the predicted mask, the frozen VAE decoder maps back to the pixel space. This produces a 3-channel output, which we subsequently average across the channels to obtain the final single-channel predicted segmentation mask.

Adapting U-Net. To adapt U-Net to the input of the support and query latent, we introduced an additional input convolutional layer for cascading features from the support set, following the approach of [17].

3.3. Support-Query Interaction

As illustrated in Fig. 2, the Support-Query Interaction (SQI) module facilitates the integration of support set information into the query feature processing pipeline. We begin by encoding the support set (image I^s , mask M^s) and the query set (image I^q , mask M^q) using the frozen VAE

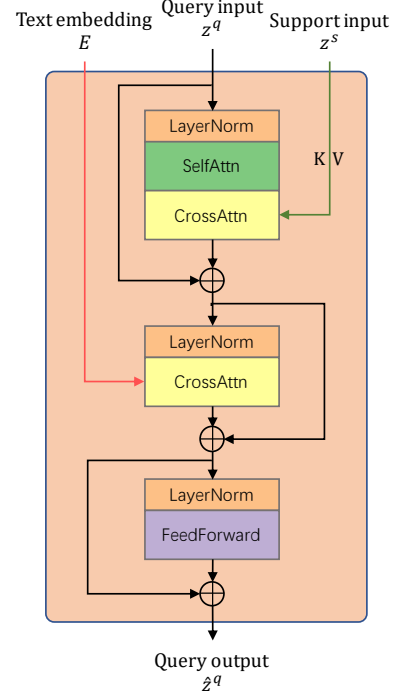


Figure 3. Modified BasicTransformerBlocks architecture.

encoder \mathcal{E} to obtain their corresponding latent representations $z \in \mathbb{R}^{1 \times c \times h \times w}$. Specifically, we denote these as z^{si} (support image latent), z^{sm} (support mask latent), and z^{qi} (query image latent). The z^{si} and z^{sm} are concatenated channel-wise to form the combined support latent $z^s = \text{concat}(z^{si}, z^{sm})$, which serves as input for the U-Net.

Support Information Injection (SII). The U-Net in Stable Diffusion utilizes *BasicTransformerBlocks* for integrating conditional information (typically text embedding) with image features. Each block sequentially applies self-attention (SAttn), cross-attention (CAtn), and a feed-forward network (FFN). Inspired by the work [51], we modified this structure to inject support set information to query, as shown in Fig. 3. After the standard self-attention on the query input z^q , we introduce an additional cross-attention layer where the query input attend to the support input z^s (acting as key K and value V). This enriched query input then undergoes the original cross-attention with the text embedding E . The modified operation becomes:

$$\hat{z}^q = \text{FFN}(\text{CAtn}(\text{CAtn}(\text{SAttn}(z^q), z^s), E)). \quad (1)$$

Query Enhancement (QE). To further enhance the interaction between support and query, we employ a prototype-based query latent enhancement strategy. The architecture of the QE module is highlighted within the yellow block in Fig. 2.

First, we reference the SSP [9] method to extract the

query prototype P^q . Specifically, we compute a foreground prototype $P^s \in \mathbb{R}^{1 \times c}$ from the support set using Masked Average Pooling (MAP) on the support image latent z^{si} guided by the support mask M^s :

$$P^s = \frac{\sum_{i,j} M_{i,j}^s \odot z_{i,j}^{si}}{\sum_{i,j} M_{i,j}^s}, \quad (2)$$

where $M_{i,j}^s$ is the mask value at spatial location (i, j) , $z_{i,j}^{si}$ is the corresponding latent feature vector, \odot denotes element-wise multiplication.

Next, we compute the cosine similarity between P^s and z^{qi} to generate a probability map *prob*. We then obtain the query prototype $P^q \in \mathbb{R}^{1 \times c}$ by averaging the query latent z^{qi} for which the corresponding similarity scores *prob* exceed a threshold τ (set to 0.7 in our work):

$$P^q = \text{mean}\{z_{i,j}^{qi} \mid \text{prob}_{i,j} > \tau\}. \quad (3)$$

This query prototype P^q is expanded spatially to match the dimensions of z^{qi} , yielding $\hat{P}^q \in \mathbb{R}^{1 \times c \times h \times w}$. We concatenate this expanded query prototype with the original query image latent along the channel dimension to obtain $z^{qt} \in \mathbb{R}^{1 \times 2c \times h \times w}$:

$$z^{qt} = \text{concat}(z^{qi}, \hat{P}^q). \quad (4)$$

3.4. Visual-to-Textual Condition Translator

Prior works [51] might resort to using null text embeddings, but this provides no specific guidance and fails to leverage the model’s powerful text-conditioning mechanism. To this end, we introduce the Visual-to-Textual Condition Translator (VTCT), a module designed to act as a “visual-to-semantic” bridge. Inspired by ODISE [48], the VTCT’s goal is to convert the visual cues from the support set directly into a text-like embedding that the Stable Diffusion model can natively understand.

The architecture of the VTCT module is highlighted within the red block in Fig. 2. To effectively capture the semantic content of the support set, we first employ a pre-trained and frozen image encoder \mathcal{V} to extract features F^s from the support image I^s . Subsequently, we perform MAP using the M^s to aggregate the foreground features within F^s , yielding a class-specific prototype $P^e \in \mathbb{R}^{1 \times d_{img}}$. Here, d_{img} denotes the feature dimension of the chosen image encoder \mathcal{V} .

Finally, this prototype P^e , which encapsulates the core visual information of the support class, is fed into a learnable Multi-Layer Perceptron (MLP). This MLP projects P^e into the target embedding space required by the diffusion model’s U-Net, producing the implicit text embedding $E \in \mathbb{R}^{1 \times 1 \times d_{text}}$, where d_{text} is the dimension of the text embeddings expected by the U-Net’s cross-attention layers.

This strategy allows us to precisely steer the powerful generative priors of Stable Diffusion towards the desired

anatomy by “speaking its language,” providing content-aware guidance that is far more specific and effective than a simple null prompt.

3.5. Training Objective

Our training objective is designed to leverage the strengths of diffusion models for segmentation. In our approach, the model takes an image latent as input and processes it through a U-Net to generate a prediction. The key idea is to train the network to accurately predict the segmentation by comparing the predicted latent with the ground truth mask latent.

Specifically, we use the query mask latent z^{qm} , as the target for prediction \hat{z}^{qm} . Following the DiffewS [51], we use the Mean Squared Error (MSE) to quantify the difference between the prediction and the target. The loss function is defined as:

$$\mathcal{L} = \frac{1}{h \times w} \sum_{i=1}^h \sum_{j=1}^w (z_{i,j}^{qm} - \hat{z}_{i,j}^{qm})^2. \quad (5)$$

3.6. SD-FSMIS Inference

Fig. 4 illustrates the SD-FSMIS inference process. Specifically, the support and query sets are first encoded into latent space using the VAE encoder \mathcal{E} . The support image latent and mask latent are concatenated and fed into the U-Net to provide class information. Under the condition of the generated text embedding E , the query latent z^q is segmented in one step and decoded by the decoder \mathcal{D} into an image, with its three channels averaged to produce the final mask \hat{M}^q .

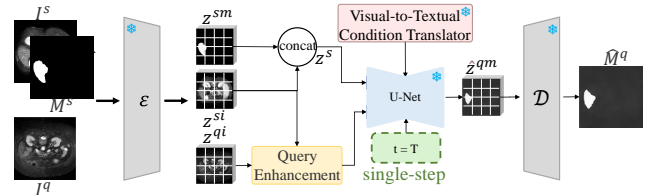


Figure 4. Overview of the SD-FSMIS inference process.

4. Experiments

4.1. Experimental Setup

Datasets. Following the evaluation protocol in RPT [52], we assess the performance of our model on Abd-MRI [16] and Abd-CT [18].

Evaluation Metric and Settings. We primarily use the Dice Similarity Coefficient (DSC) to measure segmentation accuracy, which is the standard metric for this task. All experiments are conducted in the 1-shot setting, and performance is reported as the average over a 5-fold cross-validation to ensure statistical robustness.

Table 1. Quantitative comparison (in Dice score %) of different methods under setting 1 and 2 on the Abd-MRI and Abd-CT. The best value is shown in bold font, and the second best value is underlined. As "DiffewS" was originally designed for natural images, we re-implemented and trained it on our medical datasets and protocols to ensure a direct and fair comparison.

Setting	Method	Ref.	Abd-MRI					Abd-CT				
			Spleen	Liver	LK	RK	Mean	Spleen	Liver	LK	RK	Mean
1	PANet [40]	ICCV'19	40.58	50.40	30.99	32.19	38.53	36.04	49.55	20.67	21.19	32.86
	SENet [31]	MIA'20	47.30	29.02	45.78	47.96	42.51	43.66	35.42	24.42	12.51	29.00
	SSL-ALPNet [28]	ECCV'20	72.18	76.10	81.92	85.18	78.84	70.96	78.29	72.36	71.81	73.35
	ADNet [11]	MIA'22	72.29	82.11	73.86	85.80	78.51	63.48	77.24	72.13	79.06	72.97
	AAS-DCL [44]	ECCV'22	76.24	72.33	80.37	86.11	78.76	72.30	75.41	74.69	74.18	73.66
	Q-Net [34]	IntelliSys'23	75.99	81.74	78.36	87.98	81.02	—	—	—	—	—
	RPT [52]	MICCAI'23	76.37	<u>82.86</u>	80.72	<u>89.82</u>	82.44	79.13	82.57	77.05	72.58	77.83
	CAT-Net [23]	MICCAI'23	68.83	78.98	74.01	78.90	75.18	67.65	75.31	63.36	60.05	66.59
	PAMI [53]	TMI'24	76.37	82.59	81.83	88.73	82.83	72.38	81.32	76.52	<u>80.57</u>	77.69
	PGRNet [15]	TMI'24	81.72	83.27	81.44	87.44	<u>83.47</u>	72.09	82.48	74.23	79.88	77.17
	DIFD [5]	TMI'25	75.72	80.99	88.59	91.19	84.12	<u>79.41</u>	79.66	<u>83.03</u>	78.67	<u>80.19</u>
	DiffewS* [51]	NIPS'24	76.37	78.49	75.01	87.43	79.32	78.65	80.51	74.85	80.46	78.80
Ours	—	<u>80.43</u>	78.71	<u>84.17</u>	89.34	83.16	85.01	<u>81.37</u>	83.21	85.04	83.66	
2	PANet [40]	ICCV'19	40.58	50.40	30.99	32.19	38.53	36.04	49.55	20.67	21.19	32.86
	SENet [31]	MIA'20	47.30	29.02	45.78	47.96	42.51	43.66	35.42	24.42	12.51	29.00
	SSL-ALPNet [28]	ECCV'20	67.02	73.05	73.63	78.39	73.02	60.25	73.65	63.34	54.82	63.02
	ADNet [11]	MIA'22	59.44	77.03	59.64	56.68	63.20	50.97	70.63	48.41	40.52	52.63
	AAS-DCL [44]	ECCV'22	74.86	69.94	76.90	83.75	76.36	66.36	71.61	64.71	69.95	68.16
	Q-Net [34]	IntelliSys'23	65.37	78.25	64.81	65.94	68.59	—	—	—	—	—
	RPT [52]	MICCAI'23	<u>75.46</u>	76.37	78.33	86.01	79.04	70.80	75.24	72.99	67.73	71.69
	CAT-Net [23]	MICCAI'23	67.31	75.02	75.31	83.23	75.22	66.02	80.51	68.82	64.56	70.88
	PAMI [53]	TMI'24	75.80	81.09	74.51	86.73	79.53	71.95	74.13	72.36	67.54	71.49
	DGPANet [35]	TMI'24	69.21	75.93	73.76	75.96	73.72	65.91	65.56	74.10	68.06	68.41
	DIFD [5]	TMI'25	70.96	<u>80.38</u>	85.38	90.54	81.82	<u>78.67</u>	<u>80.77</u>	84.47	<u>75.48</u>	<u>79.85</u>
	DiffewS* [51]	NIPS'24	73.11	77.16	77.41	83.47	77.79	76.84	79.57	69.70	73.62	74.93
Ours	—	77.25	78.58	<u>85.03</u>	<u>88.27</u>	82.28	83.08	82.59	<u>82.22</u>	85.10	83.25	

To evaluate the generalization capabilities of our method, we adopt two challenging cross-domain settings proposed in prior work. Setting 1: Slices containing test classes might be present in the training set, but only as un-annotated background regions. The model is trained on pseudo-masks. Setting 2: The training slices containing the test classes are removed from the dataset. This ensures model has zero exposure to the target anatomies during training, presenting a more realistic and challenging clinical scenario.

Implementation Details. Our framework is built upon the Stable Diffusion v1.5 model. Input images are resized to 256×256 , consistent with previous methods. The image encoder within VTCT module is a DINOv2-small [27]. We follow RPT [52] to generate pseudo-masks, which serve as the supervisory signal for adapting the diffusion model. The model is trained for 15k iterations per fold on a single NVIDIA A6000 GPU, with a total training time of approximately 6 hours per fold and a memory footprint of roughly 18GB. We employ the AdamW optimizer with a weight decay of $1e-2$ and a batch size of 1. The U-Net is trained with a learning rate of $1e-5$, while the learnable MLP layers use a higher learning rate of $5e-5$. For the diffusion process, we utilize a single-step DDIM scheduler with the timestep t set

to 999.

4.2. Comparative Analysis with State-of-the-Art

Tab. 1 shows the comparison between our proposed SD-FSMIS and the existing methods. For a complete evaluation, we also include the recent diffusion-based FSS model, DiffewS [51]. On the Abd-MRI dataset, SD-FSMIS achieves an average Dice score comparable to the intricately designed DIFD [5]. Its advantages become more pronounced on the Abd-CT dataset, surpassing the best method by 3.47% in Setting 1 and 3.4% in Setting 2. The DiffewS method employs attention mechanisms solely for the interaction between support and query sets, yet it achieves performance comparable to previously well-designed approaches by leveraging the powerful visual representations pre-learned by the diffusion model. SD-FSMIS demonstrates superior performance after adaptation, achieving an average improvement of 4.88% in Dice score compared to DiffewS. Unlike prior methods that often suffer a sharp performance degradation when moving from Setting 1 to the more stringent Setting 2, SD-FSMIS exhibits remarkable resilience. The minimal drop in scores validates its superior generalization and robustness, confirming its suitability for

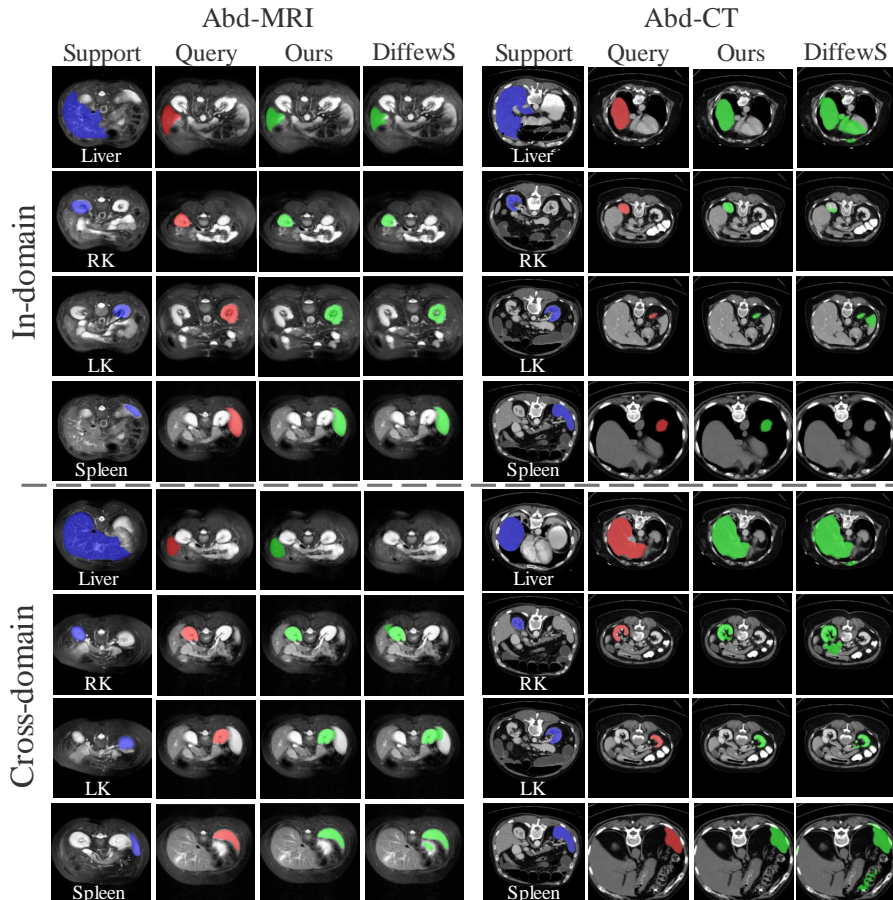


Figure 5. Qualitative comparison between our method and DiffewS method on the Abd-MRI dataset and Abd-CT dataset.

Table 2. Quantitative comparison (in Dice score %) of different cross-domain methods under setting 1. The best value is shown in bold font, and the second best value is underlined. As DiffewS was originally designed for natural images, we re-implemented and trained it on our medical datasets and protocols.

Method	Ref.	Abd-CT \rightarrow MRI					Abd-MRI \rightarrow CT				
		Spleen	Liver	LK	RK	Mean	Spleen	Liver	LK	RK	Mean
PANet [40]	ICCV'19	41.83	40.21	35.36	40.32	39.43	36.58	54.63	21.95	29.19	35.58
SSL-ALPNet [28]	ECCV'20	54.01	50.62	47.30	53.07	51.25	39.23	60.80	33.01	38.24	42.82
RPT [52]	MICCAI'23	54.94	52.58	42.58	58.44	52.13	52.04	59.47	40.29	49.60	50.35
DR-Adapter [37]	CVPR'24	53.91	62.79	71.67	74.12	65.62	55.77	70.83	55.93	44.20	56.68
IFA _{T=3} [26]	CVPR'24	59.14	67.04	73.90	75.37	68.86	56.44	71.50	54.60	50.85	58.35
FAMNet [3]	AAAI'25	58.21	73.01	57.28	74.68	65.79	65.78	73.57	57.79	61.89	64.75
DIFD [5]	TMI'25	61.05	68.29	75.51	79.69	71.14	62.45	73.86	56.86	46.88	60.01
DiffewS [51]	NIPS'24	<u>71.85</u>	74.84	<u>77.83</u>	83.86	77.09	71.06	80.39	<u>70.12</u>	66.28	71.96
Ours	—	74.70	75.26	84.77	90.96	81.42	77.78	81.02	73.03	71.72	75.90

challenging and unpredictable medical scenarios.

Recent studies have focused on the more challenging cross-domain FSMIS (CD-FSMIS) setting, which aims to develop a universal model capable of generalizing across significant domain shifts (e.g., from CT to MRI). Under this challenging setting, our method demonstrates superior

generalization capability, as shown in Tab. 2. The performance gap shown in our results can be attributed to a fundamental difference in paradigms. Conventional methods learn representations confined to their limited, relatively homogeneous training data, making their learned priors fragile when facing a new domain. In contrast, SD-FSMIS

taps into the vast and diverse visual knowledge encapsulated within the Stable Diffusion model. Its understanding of fundamental concepts like shape, texture, and context is modality-agnostic. Our proposed adaptation modules, SQI and VTCT, are the key to effectively steering this powerful, pre-existing knowledge to the specific anatomical target, resulting in a model that is inherently more robust and adaptable. This empirically validates that shifting the paradigm from designing from scratch to effectively adapting is a more promising path for solving the challenges of medical image segmentation. Additional results compared with universal models [4, 43, 45] are provided in the supplementary material.

4.3. Ablation Study and Visualizations

Effect of Each Component. We conducted a detailed ablation study to dissect the individual contributions of our framework’s key components, as shown in Tab. 3. We first establish a strong baseline by adapting the pre-trained diffusion model using only the SII module. This minimal adaptation, by itself, already achieves performance comparable to existing state-of-the-art methods, demonstrating the immense untapped potential of diffusion model priors for the FSMIS task. Building on the SII baseline, we integrated the VTCT. This single addition yielded a significant performance increase of 3.06% in the average Dice score. This confirms that translating visual support cues into text-like conditioning signals is a highly effective strategy for precisely steering the model’s generative process. Similarly, when adding the QE module to the baseline, we observed a 2.16% improvement. This highlights the importance of facilitating a deeper, more effective fusion of support and query information within the latent space. Finally, our complete SD-FSMIS framework, which integrates all components, achieves the highest average Dice score of 83.66%. This represents a 3.47% gain over the previous state-of-the-art, clearly demonstrating a powerful synergistic effect where each module complements the others to maximize performance.

Table 3. Ablative results of various components of the proposed method on the Abd-CT dataset under setting 1.

SII	QE	VTCT	Spleen	Liver	LK	RK	Mean
✓			85.54	81.86	71.72	81.31	80.11
✓		✓	83.00	82.83	<u>81.39</u>	85.45	<u>83.17</u>
✓	✓		83.74	<u>81.97</u>	80.23	83.36	82.27
✓	✓	✓	<u>85.01</u>	81.37	83.21	<u>85.04</u>	83.66

Version Comparative Analysis. We also evaluated the performance of different versions of the SD model as the backbone for our SD-FSMIS framework. Tab. 4 show that SD 1.5 yields superior performance compared to SD 2.1 in our

Table 4. Comparison of different versions of Stable Diffusion on the Abd-CT dataset under setting 1.

Version	Spleen	Liver	LK	RK	Mean
SD-1.5	85.01	81.37	83.21	85.04	83.66
SD-2.1	83.11	83.02	80.01	85.21	82.84

task. We attribute this to their distinct pre-training schemes. The broader, less-filtered dataset used for SD 1.5 appears to provide more generalizable visual priors that, after our adaptation, are better suited for the structural and textural features found in medical scans. In contrast, the heavily filtered dataset and different text encoder of SD 2.1 may result in priors that are less aligned with this specific downstream task. Consequently, we selected SD 1.5 as the default backbone for all our main experiments to ensure optimal performance.

Visualization of results. To further demonstrate the effectiveness of our method, Fig. 5 presents visualization results of the predictions from SD-FSMIS on the Abd-MRI and Abd-CT datasets under Setting 1. The results clearly show that our SD-FSMIS generates high-quality segmentation masks for organs with varying intensities, scales, and morphologies, even in complex backgrounds. Furthermore, our model produces high-quality segmentation results even when applied to the more challenging cross-domain FSMIS tasks.

5. Conclusion

In this work, we proposed SD-FSMIS, a novel approach that leverages Stable Diffusion for the FSMIS task. To adapt the SD model for FSMIS, we introduced a Support-Query Interaction module that facilitates effective information exchange between support and query. Additionally, we proposed a Visual-to-Textual Condition Translator module to harness the prior knowledge of the SD model by learning text-like embeddings from the support to guide query segmentation. Experiments on Abd-MRI, and Abd-CT datasets demonstrate that SD-FSMIS achieves competitive Dice scores compared to state-of-the-art FSMIS methods. Furthermore, our cross-domain experiments validate the generalization ability and robustness of the proposed approach, yielding the best Dice performance across various scenarios.

Acknowledgments

This work was supported in part by the National Natural Science Foundation of China under Grant 62176163, Shenzhen Higher Education Stable Support Program (General Project) under Grant 20231120175215001, and Scientific Foundation for Youth Scholars of Shenzhen University.

References

- [1] Tomer Amit, Tal Shaharbany, Eliya Nachmani, and Lior Wolf. Segdiff: Image segmentation with diffusion probabilistic models. *arXiv preprint arXiv:2112.00390*, 2021. 2, 3
- [2] Dmitry Baranchuk, Ivan Rubachev, Andrey Voynov, Valentin Khruikov, and Artem Babenko. Label-efficient semantic segmentation with diffusion models. *arXiv preprint arXiv:2112.03126*, 2021. 3
- [3] Yuntian Bo, Yazhou Zhu, Lunbo Li, and Haofeng Zhang. Famnet: Frequency-aware matching network for cross-domain few-shot medical image segmentation. *arXiv preprint arXiv:2412.09319*, 2024. 7
- [4] Victor Ion Butoi, Jose Javier Gonzalez Ortiz, Tianyu Ma, Mert R Sabuncu, John Guttag, and Adrian V Dalca. Universeg: Universal medical image segmentation. In *Proceedings of the IEEE/CVF International Conference on Computer Vision*, pages 21438–21451, 2023. 8
- [5] Zimeng Cheng, Shidong Wang, Yang Long, Tao Zhou, Haofeng Zhang, and Ling Shao. Dual interspersion and flexible deployment for few-shot medical image segmentation. *IEEE Transactions on Medical Imaging*, 2025. 2, 6, 7
- [6] Prafulla Dhariwal and Alexander Nichol. Diffusion models beat gans on image synthesis. *Advances in neural information processing systems*, 34:8780–8794, 2021. 2
- [7] Hao Ding, Changchang Sun, Hao Tang, Dawen Cai, and Yan Yan. Few-shot medical image segmentation with cycle-remembrance attention. In *Proceedings of the IEEE/CVF winter conference on applications of computer vision*, pages 2488–2497, 2023. 3
- [8] Nanqing Dong and Eric P Xing. Few-shot semantic segmentation with prototype learning. In *BMVC*, page 4, 2018. 2
- [9] Qi Fan, Wenjie Pei, Yu-Wing Tai, and Chi-Keung Tang. Self-support few-shot semantic segmentation. In *European Conference on Computer Vision*, pages 701–719. Springer, 2022. 4
- [10] Ruiwei Feng, Xiangshang Zheng, Tianxiang Gao, Jintai Chen, Wenzhe Wang, Danny Z Chen, and Jian Wu. Interactive few-shot learning: Limited supervision, better medical image segmentation. *IEEE Transactions on Medical Imaging*, 40(10):2575–2588, 2021. 3
- [11] Stine Hansen, Srishti Gautam, Robert Jenssen, and Michael Kampffmeyer. Anomaly detection-inspired few-shot medical image segmentation through self-supervision with super-voxels. *Medical Image Analysis*, 78:102385, 2022. 3, 4, 6
- [12] Kaiming He, Xiangyu Zhang, Shaoqing Ren, and Jian Sun. Deep residual learning for image recognition. In *Proceedings of the IEEE conference on computer vision and pattern recognition*, pages 770–778, 2016. 1
- [13] Weizhao He, Yang Zhang, Wei Zhuo, Linlin Shen, Jiaqi Yang, Songhe Deng, and Liang Sun. Apsseg: Auto-prompt network for cross-domain few-shot semantic segmentation. In *Proceedings of the IEEE/CVF Conference on Computer Vision and Pattern Recognition*, pages 23762–23772, 2024. 1
- [14] Eric Hedlin, Gopal Sharma, Shweta Mahajan, Hossam Isack, Abhishek Kar, Andrea Tagliasacchi, and Kwang Moo Yi. Unsupervised semantic correspondence using stable diffusion. *Advances in Neural Information Processing Systems*, 36:8266–8279, 2023. 2, 3
- [15] Wendong Huang, Jinwu Hu, Junhao Xiao, Yang Wei, Xiuli Bi, and Bin Xiao. Prototype-guided graph reasoning network for few-shot medical image segmentation. *IEEE Transactions on Medical Imaging*, 2024. 6
- [16] A Emre Kavur, N Sinem Gezer, Mustafa Barış, Sinem Aslan, Pierre-Henri Conze, Vladimir Groza, Duc Duy Pham, Soumick Chatterjee, Philipp Ernst, Savaş Özkan, et al. Chaos challenge-combined (ct-mr) healthy abdominal organ segmentation. *Medical image analysis*, 69:101950, 2021. 5
- [17] Bingxin Ke, Anton Obukhov, Shengyu Huang, Nando Metzger, Rodrigo Caye Daudt, and Konrad Schindler. Repurposing diffusion-based image generators for monocular depth estimation. In *Proceedings of the IEEE/CVF Conference on Computer Vision and Pattern Recognition*, pages 9492–9502, 2024. 4
- [18] Bennett Landman, Zhoubing Xu, Juan Igelsias, Martin Styner, Thomas Langerak, and Arno Klein. Miccai multi-atlas labeling beyond the cranial vault—workshop and challenge. In *Proc. MICCAI multi-atlas labeling beyond cranial vault—workshop challenge*, page 12. Munich, Germany, 2015. 5
- [19] Chunbo Lang, Gong Cheng, Binfei Tu, and Junwei Han. Learning what not to segment: A new perspective on few-shot segmentation. In *Proceedings of the IEEE/CVF conference on computer vision and pattern recognition*, pages 8057–8067, 2022. 2
- [20] Hsin-Ying Lee, Hung-Yu Tseng, and Ming-Hsuan Yang. Exploiting diffusion prior for generalizable dense prediction. In *Proceedings of the IEEE/CVF Conference on Computer Vision and Pattern Recognition*, pages 7861–7871, 2024. 3
- [21] Alexander C Li, Mihir Prabhudesai, Shivam Duggal, Ellis Brown, and Deepak Pathak. Your diffusion model is secretly a zero-shot classifier. In *Proceedings of the IEEE/CVF International Conference on Computer Vision*, pages 2206–2217, 2023. 3
- [22] Tianyu Lin, Zhiguang Chen, Zhonghao Yan, Weijiang Yu, and Fudan Zheng. Stable diffusion segmentation for biomedical images with single-step reverse process. In *International Conference on Medical Image Computing and Computer-Assisted Intervention*, pages 656–666. Springer, 2024. 1, 3
- [23] Yi Lin, Yufan Chen, Kwang-Ting Cheng, and Hao Chen. Few shot medical image segmentation with cross attention transformer. In *International Conference on Medical Image Computing and Computer-Assisted Intervention*, pages 233–243. Springer, 2023. 6
- [24] Grace Luo, Lisa Dunlap, Dong Huk Park, Aleksander Holynski, and Trevor Darrell. Diffusion hyperfeatures: Searching through time and space for semantic correspondence. *Advances in Neural Information Processing Systems*, 36:47500–47510, 2023. 3
- [25] Xusen Ma, Xiaoqin Wang, Xianxu Hou, Meidan Ding, Zhe Kong, Junliang Chen, and Linlin Shen. Ospa: Enhancing identity-preserving image generation via online self-preference alignment. 2

- [26] Jiahao Nie, Yun Xing, Gongjie Zhang, Pei Yan, Aoran Xiao, Yap-Peng Tan, Alex C Kot, and Shijian Lu. Cross-domain few-shot segmentation via iterative support-query correspondence mining. In *Proceedings of the IEEE/CVF Conference on Computer Vision and Pattern Recognition*, pages 3380–3390, 2024. 7
- [27] Maxime Oquab, Timothée Darcet, Théo Moutakanni, Huy Vo, Marc Szafranec, Vasil Khalidov, Pierre Fernandez, Daniel Haziza, Francisco Massa, Alaaeldin El-Nouby, et al. Dinov2: Learning robust visual features without supervision. *arXiv preprint arXiv:2304.07193*, 2023. 1, 6
- [28] Cheng Ouyang, Carlo Biffi, Chen Chen, Turkay Kart, Huaqi Qiu, and Daniel Rueckert. Self-supervision with superpixels: Training few-shot medical image segmentation without annotation. In *European conference on computer vision*, pages 762–780. Springer, 2020. 3, 6, 7
- [29] Bastien Rigaud, Brian M Anderson, H Yu Zhiqian, Maxime Gobeli, Guillaume Cazoulat, Jonas Söderberg, Elin Samuelsson, David Lidberg, Christopher Ward, Nicolette Taku, et al. Automatic segmentation using deep learning to enable online dose optimization during adaptive radiation therapy of cervical cancer. *International Journal of Radiation Oncology* Biology* Physics*, 109(4):1096–1110, 2021. 1
- [30] Robin Rombach, Andreas Blattmann, Dominik Lorenz, Patrick Esser, and Björn Ommer. High-resolution image synthesis with latent diffusion models. In *Proceedings of the IEEE/CVF conference on computer vision and pattern recognition*, pages 10684–10695, 2022. 2, 3
- [31] Abhijit Guha Roy, Shayan Siddiqui, Sebastian Pölsterl, Nassir Navab, and Christian Wachinger. ‘squeeze & excite’ guided few-shot segmentation of volumetric images. *Medical image analysis*, 59:101587, 2020. 3, 6
- [32] Christoph Schuhmann, Romain Beaumont, Richard Vencu, Cade Gordon, Ross Wightman, Mehdi Cherti, Theo Coombes, Aarush Katta, Clayton Mullis, Mitchell Wortsman, et al. Laion-5b: An open large-scale dataset for training next generation image-text models. *Advances in neural information processing systems*, 35:25278–25294, 2022. 2, 3
- [33] Amirreza Shaban, Shray Bansal, Zhen Liu, Irfan Essa, and Byron Boots. One-shot learning for semantic segmentation. *arXiv preprint arXiv:1709.03410*, 2017. 2
- [34] Qianqian Shen, Yanan Li, Jiyong Jin, and Bin Liu. Q-net: Query-informed few-shot medical image segmentation. In *Proceedings of SAI Intelligent Systems Conference*, pages 610–628. Springer, 2023. 3, 6
- [35] Yue Shen, Wanshu Fan, Cong Wang, Wenfei Liu, Wei Wang, Qiang Zhang, and Dongsheng Zhou. Dual-guided prototype alignment network for few-shot medical image segmentation. *IEEE Transactions on Instrumentation and Measurement*, 2024. 6
- [36] Michael V Sherer, Diana Lin, Sharif Elguindi, Simon Duke, Li-Tee Tan, Jon Cacicedo, Max Dafele, and Erin F Gillespie. Metrics to evaluate the performance of auto-segmentation for radiation treatment planning: A critical review. *Radiotherapy and Oncology*, 160:185–191, 2021. 1
- [37] Jiapeng Su, Qi Fan, Wenjie Pei, Guangming Lu, and Fanglin Chen. Domain-rectifying adapter for cross-domain few-shot segmentation. In *Proceedings of the IEEE/CVF Conference on Computer Vision and Pattern Recognition*, pages 24036–24045, 2024. 7
- [38] Luming Tang, Menglin Jia, Qianqian Wang, Cheng Perng Phoo, and Bharath Hariharan. Emergent correspondence from image diffusion. *Advances in Neural Information Processing Systems*, 36:1363–1389, 2023. 3
- [39] Zhuotao Tian, Hengshuang Zhao, Michelle Shu, Zhicheng Yang, Ruiyu Li, and Jiaya Jia. Prior guided feature enrichment network for few-shot segmentation. *IEEE transactions on pattern analysis and machine intelligence*, 44(2):1050–1065, 2020. 2
- [40] Kaixin Wang, Jun Hao Liew, Yingtian Zou, Daquan Zhou, and Jiashi Feng. Panet: Few-shot image semantic segmentation with prototype alignment. In *proceedings of the IEEE/CVF international conference on computer vision*, pages 9197–9206, 2019. 2, 3, 6, 7
- [41] Xiaoqin Wang, Xianxu Hou, Meidan Ding, Junliang Chen, Kaijun Deng, Jinheng Xie, and Linlin Shen. Disfacerep: Representation disentanglement for co-occurring facial components in weakly supervised face parsing. In *Proceedings of the 33rd ACM International Conference on Multimedia*, pages 4020–4029, 2025. 1
- [42] Xiaoqin Wang, Xusen Ma, Xianxu Hou, Meidan Ding, Yudong Li, Junliang Chen, Wenting Chen, Xiaoyang Peng, and Linlin Shen. Facebench: A multi-view multi-level facial attribute vqa dataset for benchmarking face perception mllms. In *Proceedings of the Computer Vision and Pattern Recognition Conference*, pages 9154–9164, 2025. 1
- [43] Hallee E Wong, Jose Javier Gonzalez Ortiz, John Guttag, and Adrian V Dalca. Multiverseg: scalable interactive segmentation of biomedical imaging datasets with in-context guidance. In *Proceedings of the IEEE/CVF International Conference on Computer Vision*, pages 20966–20980, 2025. 8
- [44] Huisi Wu, Fangyan Xiao, and Chongxin Liang. Dual contrastive learning with anatomical auxiliary supervision for few-shot medical image segmentation. In *European Conference on Computer Vision*, pages 417–434. Springer, 2022. 6
- [45] Junde Wu and Min Xu. One-prompt to segment all medical images. In *Proceedings of the IEEE/CVF conference on computer vision and pattern recognition*, pages 11302–11312, 2024. 8
- [46] Junde Wu, Rao Fu, Huihui Fang, Yu Zhang, Yehui Yang, Haoyi Xiong, Huiying Liu, and Yanwu Xu. Medsegdiff: Medical image segmentation with diffusion probabilistic model. In *Medical Imaging with Deep Learning*, pages 1623–1639. PMLR, 2024. 3
- [47] Junde Wu, Wei Ji, Huazhu Fu, Min Xu, Yueming Jin, and Yanwu Xu. Medsegdiff-v2: Diffusion-based medical image segmentation with transformer. In *Proceedings of the AAAI conference on artificial intelligence*, pages 6030–6038, 2024. 3
- [48] Jiarui Xu, Sifei Liu, Arash Vahdat, Wonmin Byeon, Xiaolong Wang, and Shalini De Mello. Open-vocabulary panoptic segmentation with text-to-image diffusion models. In *Proceedings of the IEEE/CVF Conference on Computer Vi-*

- sion and Pattern Recognition*, pages 2955–2966, 2023. [3](#), [5](#)
- [49] Jiarui Xu, Sifei Liu, Arash Vahdat, Wonmin Byeon, Xiaolong Wang, and Shalini De Mello. Open-vocabulary panoptic segmentation with text-to-image diffusion models. In *Proceedings of the IEEE/CVF Conference on Computer Vision and Pattern Recognition*, pages 2955–2966, 2023. [2](#), [3](#)
- [50] Junyi Zhang, Charles Herrmann, Junhwa Hur, Luisa Polania Cabrera, Varun Jampani, Deqing Sun, and Ming-Hsuan Yang. A tale of two features: Stable diffusion complements dino for zero-shot semantic correspondence. *Advances in Neural Information Processing Systems*, 36:45533–45547, 2023. [2](#), [3](#)
- [51] Muzhi Zhu, Yang Liu, Zekai Luo, Chenchen Jing, Hao Chen, Guangkai Xu, Xinlong Wang, and Chunhua Shen. Unleashing the potential of the diffusion model in few-shot semantic segmentation. *Advances in Neural Information Processing Systems*, 37:42672–42695, 2024. [1](#), [3](#), [4](#), [5](#), [6](#), [7](#)
- [52] Yazhou Zhu, Shidong Wang, Tong Xin, and Haofeng Zhang. Few-shot medical image segmentation via a region-enhanced prototypical transformer. In *International Conference on Medical Image Computing and Computer-Assisted Intervention*, pages 271–280. Springer, 2023. [2](#), [5](#), [6](#), [7](#)
- [53] Yazhou Zhu, Shidong Wang, Tong Xin, Zheng Zhang, and Haofeng Zhang. Partition-a-medical-image: Extracting multiple representative sub-regions for few-shot medical image segmentation. *IEEE Transactions on Instrumentation and Measurement*, 2024. [6](#)